Atomic and magnetic short-range order in Ag-Mn spin-glass alloys

Kenji Koga and Ken-ichi Ohshima
Institute of Applied Physics, University of Tsukuba, Tsukuba 305, Japan

Nobuo Niimura
Laboratory of Nuclear Science, Tohoku University, Sendai 982, Japan
(Received 20 March 1992; revised manuscript received 2 October 1992)

To understand the relationship between the magnetic properties and local arrangements of Mn spins in Ag-Mn spin-glass alloys, we have measured the magnetic susceptibility, and x-ray and diffuse-neutron-scattering intensities for three single crystals. The x-ray results show that the Mn atoms are found to have a preference for linking up along ⟨100⟩ directions. This tendency increases with increasing Mn content up to around 20.8 at. % Mn. However, this tendency decreases abruptly at 28.1 at. % Mn. The neutron results for the spin-glass state of Ag-20.8 at. % Mn alloy show that the nearest spin pairs have strong antiferromagnetic coupling and the second-nearest spin pairs along the ⟨100⟩ directions are correlated ferromagnetically with each other. These ferromagnetic spin chains are found to develop inside the atomic short-range-ordered region of Mn atoms. In addition to the existence of these spin chains, we have also observed longer-range spin correlation with about twice the correlation length of the atomic one. The amplitude of the magnetic susceptibility at the freezing temperature and the paramagnetic Curie temperature are found to have a strong relationship with the short-range spin structure. We believe that the longer-range spin correlations cannot grow without conflicting with the short-range spin structures inside the atomic short-range-ordered region of Mn atoms. This may become a key point to understand the spin-glass freezing mechanism.

I. INTRODUCTION

Spin-glass is characterized by the imperfect periodicity of magnetic atoms from a structural aspect, which yields the disordered spin arrangements at low temperature. Although the spins fail to form magnetic long-range order even at low temperatures, they are known to form magnetic short-range order (MSRO), which is believed to be derived from the atomic short-range order (ASRO) of magnetic atoms. However, this detailed relationship is still not clear. MSRO has information about how spins are correlated with each other in the disordered media and fall into the spin-glass state. Moreover, it is important for the spin-glass study to investigate the relationship between the macroscopic magnetic behavior and MSRO.

The most simple spin-glass systems are noble-metal alloys containing $3d$ transition metals (Cr, Mn, and Fe). The Ag-Mn alloy is regarded as a typical spin-glass system similar to the Cu-Mn alloy, though the former has not been studied as much as the latter. Kouvel[1] has found a spin-glass-type freezing for fcc Ag-Mn alloys with Mn content from 10 to 25 at. % by using a magnetic susceptibility technique. Bouchiat *et al.*[2] have observed diffuse maxima at the 1,0.5,0 and its equivalent positions in the x-ray photographic plates and performed the small-angle x-ray scattering experiments for several Ag-Mn alloys. They proposed two possible models based on the space group $I4_1/amd$ from the diffuse intensity patterns: (1) heterogeneous model where the alloy contains microdomains of stoichiometric AgMn and (2) homogeneous model where the alloy presents sinusoidal composition fluctuations. However, a conclusive description was not obtained from their experiments. They also briefly discussed the magnetic implication of the model in view of the known spin-glass parameters. Bouchiat and Dartyge[3] measured the small-angle x-ray scattering at a smaller angle from the Ag-Mn alloys and found no diffuse scattering signal except for the Laue monotonic background intensity, from which they rejected the above two models and employed the homogeneous distribution of Mn atoms. They have analyzed the x-ray diffuse intensities from the shaded patterns on the photographic plates and calculated several ASRO parameters approximately. Extended x-ray-absorption fine structure (EXAFS) studies[4] also supported their x-ray scattering results, where the first-nearest-neighbor ASRO parameter was determined.

In the early neutron-scattering studies on the spin-glass alloys, Wells and Smith[5] measured the atomic and magnetic diffuse scattering from Cu-Mn single crystals and determined several ASRO and MSRO parameters. Werner and Cable[6] and Cable *et al.*[7,8] observed the magnetic diffuse maxima at $1,0.5\pm\delta,0$ positions on the $(hk0)$ reciprocal-lattice plane and found the concentration dependence of these positions and the temperature dependence of their amplitudes. They interpreted the origin of the diffuse maxima as an incommensurate spin modulation stabilized by Ruderman-Kittel-Kasuya-Yoshida (RKKY) interactions. They also found the ferromagnetic clusters associated with the ASRO, which coexisted with the incommensurate modulated regions. They thought

that the interactions between ferromagnetic clusters and modulated regions are important to the understanding of spin-glass behavior. On the other hand, Ishibashi *et al.*[9] carried out a neutron-scattering experiment on Ag-Mn alloys and found similar magnetic diffuse maxima to that found in Cu-Mn alloys along the $[1,k,0]$ directions. They measured the temperature dependence and could not find any anomalies around the freezing temperature. The diffuse peak positions of the Ag-Mn alloys were found to coincide with those of the Cu-Mn alloys with the same Mn contents even though lattice spacing for the former alloys are about 10% longer than that for the latter ones. From these results, they suggested that the diffuse maxima have come from a Fermi surface effect via RKKY interactions, which was pointed out by Harder and Wells.[10] Werner, Rhyne, and Gotaas[11] performed high-resolution inelastic-neutron-scattering measurements on a Cu-Mn alloy at the magnetic diffuse peak position. They found that the pure elastic scattering has started to increase below the freezing temperature T_g and the inelastic components show cusplike behavior near T_g. The origin of diffuse maxima has been considered as the incomplete development of long-range spin density waves due to the disordered arrangements of Mn atoms.

Owing to the lack of quantitative measurements for the Ag-Mn alloys compared with Cu-Mn, there are many uncertainties in the relationship between magnetic properties and local spin arrangements. In this paper, we have undertaken x-ray diffuse and neutron magnetic diffuse scattering measurements on the Ag-Mn alloys, which provide evidence of two different coexisting correlations. One is the ferromagnetic spin chains along ⟨100⟩ directions existing in the local structure of Mn atoms, which are coupled antiferromagnetically by the first-nearest-neighbor bonds, in contrast with the Cu-Mn alloys possessing ferromagnetic clusters. The other is the longer-range spin correlations which are exhibited, similar to that in the Cu-Mn alloys. We believe that an inevitable competition would arise between the short-range spin structures and the longer-range spin correlations inside the local structures of Mn atoms, which may be an intrinsic feature of the spin-glass freezing.

II. SAMPLE PREPARATION

Silver-rich Ag-Mn alloy is known to possess a fcc disordered region up to 47 at. % Mn and show a phase segregation of αMn or βMn at the low-temperature region, from the atomic phase diagram.[12] Three single crystals with different compositions were grown by the Bridgman technique in a ZrO_2 crucible, where the purity of the starting materials was 99.99% for Ag and Mn. All specimens were homogenized at 850 °C for several hours and quenched into ice brine to avoid the phase segregation. Platelike samples of about 10 mm in diameter and 3mm thick were cut from the ingots for x-ray studies. These surface were parallel to the (210) planes. A cylindrical sample (Ag-20.8 at. % Mn) of 7 mm in diameter and 16 mm height for neutron study was cut from the same ingot. The cylindrical direction was set to [001]. Rectangular samples of $5\times5\times1$ mm^3 for magnetic measurements were also cut from the same ingots. They were chemically etched with 50% nitric acid and 50% distilled water at 5 °C to remove the distorted surface layer.

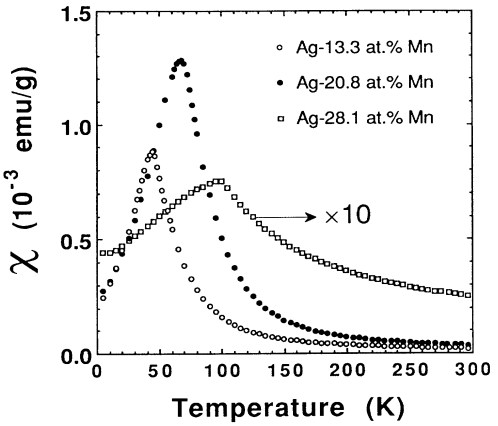

FIG. 1. Temperature dependence of dc magnetic susceptibility of Ag-13.3 (○), Ag-20.8 (●), and Ag-28.1 (□) at. % Mn alloys measured by a SQUID in a 100-Oe field under zero field cooling.

The compositions were estimated with electron probe microanalysis (EPMA) to be Ag-13.3±0.3, Ag-20.8±0.3, and Ag-28.1±0.5 at. % Mn.

III. MAGNETIC-SUSCEPTIBILITY MEASUREMENTS

A superconducting quantum interference device (SQUID) was used to determine the following parameters: (1) paramagnetic Curie temperature Θ, (2) the effective Bohr magneton P_{eff}, (3) the spin angular momentum S, (4) the deviating temperature (from the Curie-Weiss law) T_0, and (5) the peak value of magnetic susceptibility (at the freezing temperature) $\chi(T_g)$. The low-field ac magnetic-susceptibility method was also used to determine the freezing temperature T_g precisely, which makes the cusp shape sharp.

Figure 1 shows dc magnetic susceptibilities of Ag-13.3,

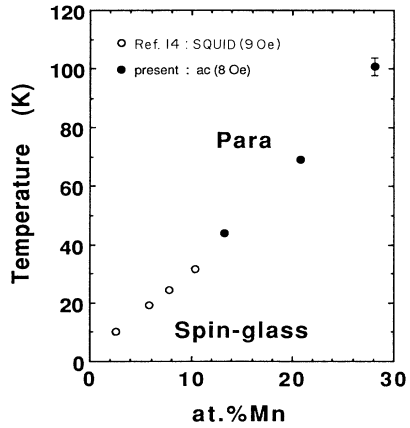

FIG. 2. The partial magnetic phase diagram of Ag-Mn alloys with the present results (●) by the ac magnetic susceptibility, and the SQUID measurements by Mozurkewich *et al.* (Ref. 14) (○).

TABLE I. The paramagnetic Curie temperature Θ, the effective Bohr magneton P_{eff}, the spin angular momentum S, the deviating temperature (from the Curie-Weiss law) T_0, the freezing temperature T_g, and the peak value of magnetic susceptibility at T_g, $\chi(T_g)$ for Ag-13.3, Ag-20.8, and Ag-28.1 at. % Mn alloys.

at. % Mn	Θ (K)	P_{eff} (μ_B)	S	T_0 (K)	T_g (K)	$\chi(T_g)$ (emu/g)
13.3	74.3	5.40	2.25	150±5	44±0.5	8.8×10^{-4}
20.8	105.7	5.04	2.07	165±5	69±0.5	1.3×10^{-3}
28.1	−39.6	4.87	1.99	235±10	103±3	7.5×10^{-5}

Ag-20.8, and Ag-28.1 at. % Mn alloys measured by a SQUID in a 100-Oe field. Table I shows the physical values of magnetization described above. There are several remarks on this table. The values of paramagnetic Curie temperature Θ for Ag-13.3 and Ag-20.8 at. % Mn alloys are positive, which indicates that the ferromagnetic interactions have more influence on the Mn spins bonds in the crystal. On the other hand, Θ for Ag-28.1 at. % Mn alloy is negative, which indicates antiferromagnetic interactions are more influential. T_g increases with increasing Mn content, but the value of $\chi(T_g)$ for Ag-28.1 at. % Mn alloy shows a very small value compared with that of the others. We will discuss the origin of this small $\chi(T_g)$ value in a later section. S is found to be fairly insensitive to the different Mn contents and to be close to 2.0, which is similar to the Cu-Mn alloys.[5,13] We summarized the partial magnetic phase diagram for the Ag-Mn alloy in Fig. 2, where the results of Mozurkewich *et al.*[14] were considered. It shows the same linearlike nature as that of the Cu-Mn alloy[15] except for the difference of its gradient.

IV. X-RAY EXPERIMENTS AND RESULTS

A. X-ray intensity measurements and analyses

X-ray intensity measurements were made by using a four-circle goniometer attached to a rotating-unit x-ray generator (Rigaku RU-300). The incident beam, Cu $K\alpha$ radiation from a Cu target, was monochromatized by a singly bent highly oriented pyrolytic graphite (HOPG) (graphite) crystal. A HOPG crystal was also used as the analyzer crystal in front of a NaI(Tl) scintillation counter to remove the Mn fluorescence from the samples.

The diffuse intensity was measured three-dimensionally by scanning the reciprocal-lattice space including the minimum volume of the first Brillouin zone at intervals of $\frac{1}{40}$, in terms of the distance between the 000 and 200 Bragg spots. The measured intensities were converted into absolute units by comparison with the intensity scattered from polystyrene (C_8H_8) at $2\theta=100°$ and integrated intensities from a powdered Al sample. The conversion factors of these two independent methods agreed within 5%. The diffuse-scattering intensity distributions on the ($hk0$) reciprocal-lattice plane from the Ag-13.3, Ag-20.8, and Ag-28.1 at. % Mn alloys are shown in Figs. 3(a), 3(b),

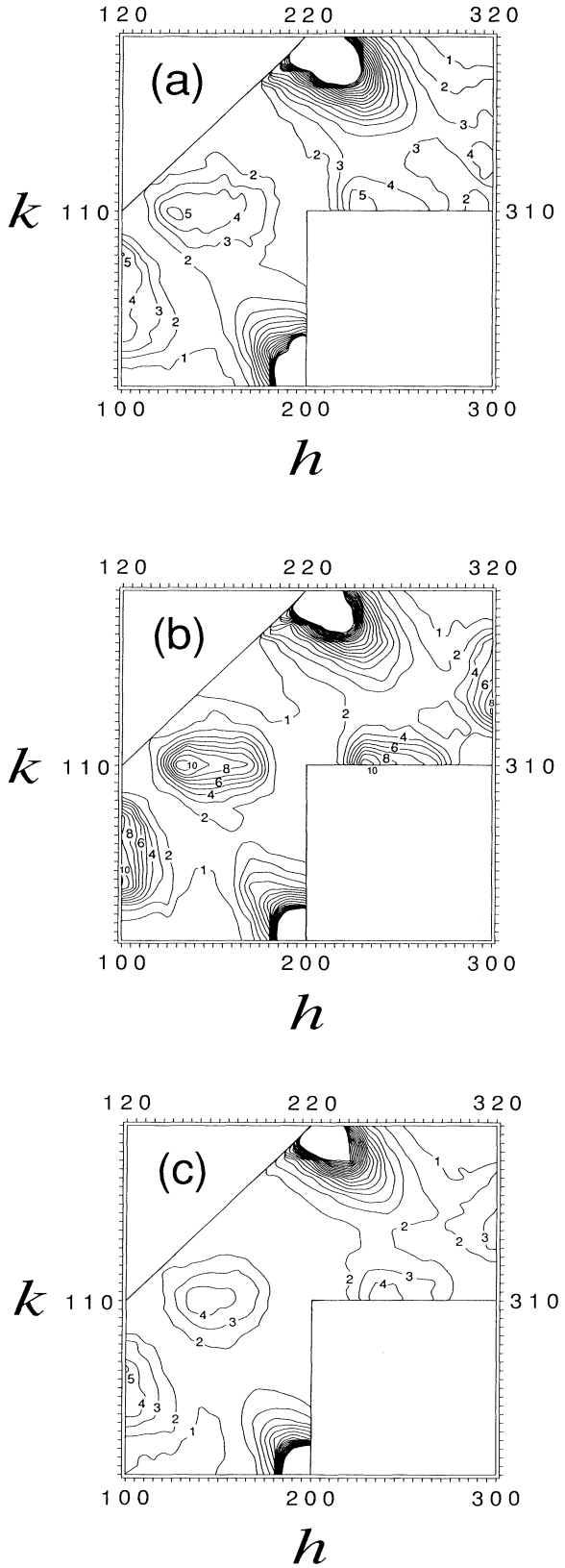

FIG. 3. Diffuse scattering intensity distributions on the ($hk0$) reciprocal-lattice plane in Laue units for (a) Ag-13.3 at. % Mn, (b) Ag-20.8 at. % Mn, and (c) Ag-28.1 at. % Mn.

and 3(c), respectively, in Laue units, where the contribution from air scattering has been subtracted. The ASRO diffuse-scattering intensity was obtained by removing the size-effect modulation, as well as Huang and thermal diffuse scattering, from the total diffuse scattering, by using the Borie and Sparks method.[16] Both Bragg intensity near the fundamental spots and the contribution from Compton scattering were also subtracted from the measured intensities. Intensity distributions due to ASRO are shown in Figs. 4(a), 4(b), and 4(c) for Ag-13.3, Ag-20.8, and Ag-28.1 at. % Mn alloys in Laue units, respectively. Every map shows the ASRO diffuse intensity around 1,0.5,0 with an elongation in the [0,1,0] direction. Diffuse maxima appeared at $1,0.25\pm0.02,0$ and its equivalent positions for the Ag-13.3 at. % Mn alloy, which were shifted to $1,0.32\pm0.02,0$ and its equivalent positions for the Ag-20.8 at. % Mn alloy. But such

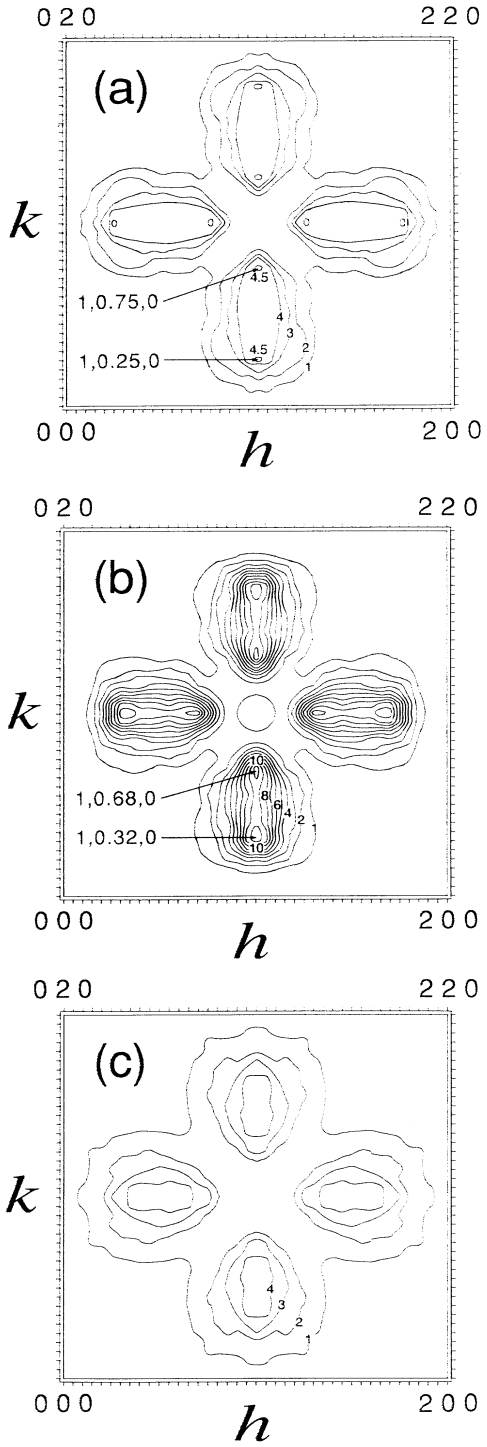

FIG. 4. The atomic short-range-order components of diffuse scattering in the ($hk0$) plane in Laue units for (a) Ag-13.3 at. % Mn, (b) Ag-20.8 at. % Mn, and (c) Ag-28.1 at. % Mn.

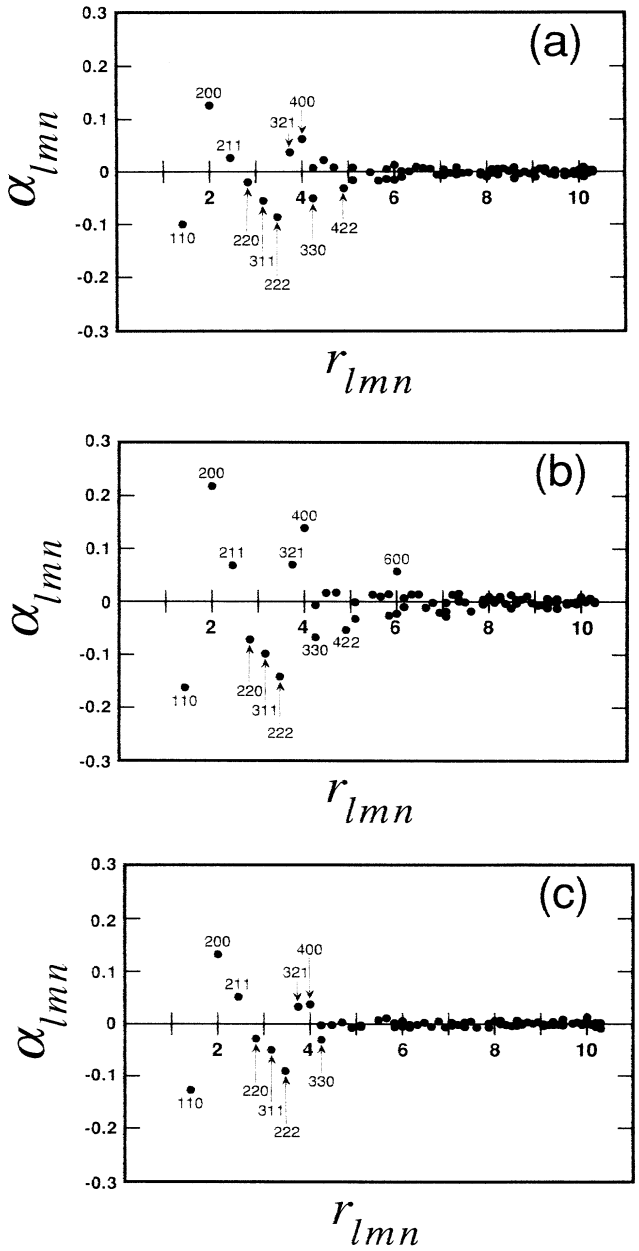

FIG. 5. Atomic short-range-order parameters α_{lmn} plotted against $r_{lmn}=(l^2+m^2+n^2)^{1/2}$ for Ag-13.3, Ag-20.8, and Ag-28.1 at. % Mn alloys, where l, m, and n are integers.

diffuse maxima were not observed for the Ag-28.1 at. % Mn alloy. The peak value of diffuse maxima increased with increasing Mn contents up to around 20.8 at. % Mn. However, it decreased abruptly at 28.1 at. % Mn.

B. ASRO parameters and local atomic arrangements

The Warren-Cowley ASRO parameters α_{lmn} up to the 50th shell were determined by the Fourier inversion of ASRO diffuse-scattering intensity for the Ag-13.3, Ag-20.8, and Ag-28.1 at. % Mn alloys, with an error estimated to be less than ±5%. These values up to the 20th shell are listed in Table II and are plotted against the atomic distance r_{lmn} $[=(l^2+m^2+n^2)^{1/2}]$ in Fig. 5, where l, m, and n are integers. α_{000} for Ag-13.3, Ag-20.8, and Ag-28.1 at. % Mn alloys has the values of 0.98, 0.95, and 0.90, respectively. For the three specimens, the local arrangement of Mn atoms has a preference for avoiding the formation of clusters due to the negative value of α_{110}. α_{200} and α_{400} are found to be all positive and obviously larger than the other parameters. We see that Mn atoms have a tendency to line up along ⟨100⟩ directions for the three samples and the linking length is largest for the Ag-20.8 at. % Mn alloy. The sign of α_{lmn} up to the 8th shell has the same tendency and the absolute value is maximum for the Ag-20.8 at. % Mn alloy. The correlation lengths of Ag-13.3, 20.8, and 28.1 at. % Mn were estimated from reconstruction of the diffuse intensity by Fourier inverse transforms of the observed ASRO parameters to be about $5a_0$, $6a_0$, and $5a_0$, respectively.

We constructed a possible local atomic arrangement by using the observed ASRO parameters and a simulation program.[17–20] The atomic arrangements in $10\times10\times10$ fcc unit cells were determined so as to adjust the α_{lmn} values from models to those from experiments up to the 30th shell for the three specimens. The results are shown in Figs. 6(a)–6(f): 6(a), 6(c), and 6(e) for the ideally random arrangements (RANDOM) of Mn atoms with 13.3 at. %, 20.8 at. %, and 28.1 at. %, respectively, in which all the parameters are fitted to be zero except for $\alpha_{000}=1$, and 6(b), 6(d), and 6(f) for the simulated ASRO structures fitted to the observed α_{lmn} values of Ag-13.3, Ag-20.8, and Ag-28.1 at. % Mn alloys, respectively. In these figures, Mn atoms are only represented by circles and they are linked together by red or green solid lines which are first- or second-nearest-neighbor bonds in a fcc lattice, respectively. In particular, we have drawn the structural models with reduction to one-eighth of original volumes ($5\times5\times5$ fcc unit cells) for easy understanding. A set of α_{lmn} parameters corresponding to the simulated structure is compared with those determined by experiment in Table II. The agreement between simulated and experimental values was estimated by a reliability factor defined as

TABLE II. Atomic short-range-order (ASRO) parameters of disordered Ag-13.3, Ag-20.8, and Ag-28.1 at. % Mn alloys determined from the Fourier transform of the ASRO diffuse-scattering intensities and those calculated from the model by computer simulation [see Figs. 6(b), 6(d), and 6(f)]. N is the shell number.

		Ag-13.3 at. % Mn		Ag-20.8 at. % Mn		Ag-28.1 at. % Mn	
N	lmn	Expt.	Model	Expt.	Model	Expt.	Model
0	000	0.976	1.000	0.947	1.000	0.902	1.000
1	110	−0.100	−0.099	−0.167	−0.159	−0.127	−0.126
2	200	0.126	0.126	0.218	0.203	0.133	0.132
3	211	0.027	0.027	0.068	0.069	0.051	0.051
4	220	−0.020	−0.019	−0.072	−0.059	−0.028	−0.028
5	310	−0.055	−0.056	−0.098	−0.096	−0.050	−0.050
6	222	−0.086	−0.087	−0.141	−0.147	−0.090	−0.090
7	321	0.037	0.036	0.069	0.065	0.033	0.033
8	400	0.062	0.063	0.139	0.143	0.037	0.038
9	330	−0.050	−0.050	−0.067	−0.069	−0.030	−0.030
	411	−0.008	−0.007	−0.006	−0.008	−0.002	−0.002
10	420	0.022	0.022	0.016	0.014	−0.002	−0.001
11	332	0.009	0.009	0.017	0.021	0.003	0.004
12	422	−0.031	−0.030	−0.053	−0.051	−0.007	−0.008
13	431	0.008	0.008	−0.001	0.002	−0.005	−0.005
	510	−0.016	−0.061	−0.032	−0.033	−0.002	−0.002
14	521	−0.001	0.000	0.013	0.015	0.008	0.008
15	440	−0.017	0.017	0.010	0.011	0.011	0.011
16	433	0.005	0.005	0.014	0.011	0.002	0.002
	530	−0.014	−0.014	−0.026	−0.025	−0.005	−0.005
17	442	−0.015	0.016	−0.022	−0.022	−0.005	−0.005
	600	0.013	0.014	0.057	0.056	0.006	0.006
18	532	0.001	0.001	0.007	0.005	−0.001	−0.002
	611	−0.010	−0.010	−0.010	−0.009	−0.007	−0.007
19	620	0.001	0.001	0.014	0.013	−0.001	−0.001
20	541	0.010	0.010	0.014	0.012	0.003	0.003

$$R=\frac{\sum_{lmn}\{\alpha_{lmn}(\text{expt.})-\alpha_{lmn}(\text{model})\}^2}{\sum_{lmn}\alpha_{lmn}^2(\text{expt.})}$$

with summing up to the 50th shell. The R values were 0.08, 0.03, and 0.02 for the above three samples, respectively. This agreement is thought to be fairly good.

The structural difference between the ASRO and RANDOM structures can be characterized quantitatively by comparing the number of first- and second-nearest Mn-Mn atom pairs and their ratios. They are given in Table III. In the ASRO structure of Ag-20.8 at. % Mn alloy [Fig. 6(d)], there are many second-nearest Mn-Mn pairs (green lines) along ⟨100⟩ directions with three-dimensional connections. They are not percolated by themselves to the infinite range, but are connected with each other through the first-nearest-neighbor bonds. The average length of chains is estimated to be three or four units cells. In the random distribution of Mn atoms with 20.8 at. % [Fig. 6(c)], there are many first neighbors (red lines) and few one-dimensional arrays along ⟨100⟩ directions. In the ASRO structure of Ag-13.3 at. % Mn [Fig. 6(b)], there are also many second-nearest Mn-Mn pairs (green lines) along ⟨100⟩ directions. Although the linking length becomes shorter one-dimensionally, which is estimated as one or two unit cells, the ratio of number of second-nearest neighbors to that of first-nearest neigh-

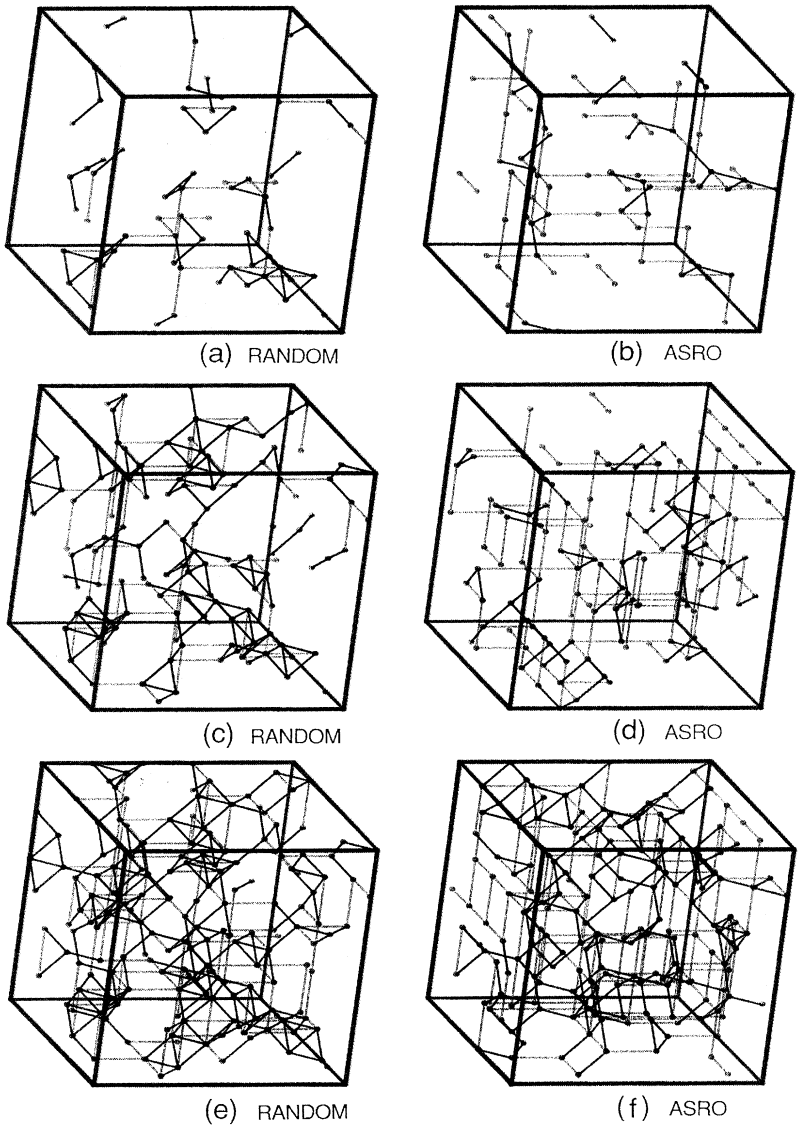

FIG. 6. Three-dimensional distribution of Mn atoms simulated on 5×5×5 fcc unit cells; (a), (c), and (e) for the ideally disordered state of Ag-13.3, Ag-20.8, and Ag-28.1 at. % Mn alloys, respectively, and (b), (d), and (f) for the observed ASRO structures of Ag-13.3, Ag-20.8, and Ag-28.1 at. % Mn alloys, respectively. Only Mn atoms are represented by circles and they are linked together by red and green solid lines which are first- and second-nearest neighbors to each other in a fcc lattice.

TABLE III. The number of Mn-Mn atom pairs in the (i) first- and (ii) second-nearest neighbors, and (iii) the ratio of the number of second-nearest neighbors to that of first-nearest ones.

	Ag-13.3 at. % Mn		Ag-20.8 at. % Mn		Ag-28.1 at. % Mn	
	RANDOM	ASRO	RANDOM	ASRO	RANDOM	ASRO
(i)	465	161	1091	436	1953	1350
(ii)	210	410	528	972	985	1350
(iii)	0.45	2.55	0.48	2.23	0.50	1.00

bors is still higher in the ASRO than in the RANDOM as indicated in Table III. On the other hand, the ASRO structure of Ag-28.1 at. % Mn [Fig. 6(f)] is closer to the random distribution [Fig. 6(e)], as the ratio of the number of second-nearest neighbors to that of first-nearest neighbors decreases abruptly as shown in Table III. Many first-nearest Mn-Mn pairs (red lines) exist in the ASRO state and connect with each other. The length of Mn chains along ⟨100⟩ directions has shortened due to the decrease of the amplitude and the correlation length of ASRO parameters in comparison with that of Ag-20.8 at. % Mn.

V. NEUTRON EXPERIMENTS AND RESULTS

A. Neutron intensity measurements and analyses

We have carried out a neutron-scattering experiment for the Ag-20.8 at. % Mn alloy using a four-circle goniometer with a refrigerator (DE201, Air Products) at the instrument FOX installed at the pulsed neutron source KENS of the National Laboratory for High Energy Physics, Tsukuba, Japan. We used the time-of-flight (TOF) method for collecting the neutron diffuse intensities, see, for example, the measurements of the ASRO diffuse intensity from a Cu-Mn alloy.[21] A ^{3}He counter with a soller slit was set up at a scattering angle $2\theta = 17°$ for the suitable measurement of the magnetic diffuse intensity. We have taken about 70 different TOF neutron spectra three-dimensionally which include the minimum volume of the first Brillouin zone. TOF neutron spectra along the [1,0.3,0] direction from the Ag-20.8 at. % Mn are shown in Fig. 7 at room temperature and 11 K. The background spectrum is also displayed in this figure, which was measured without the sample. Both spectra at room temperature and 11 K exhibit a diffuse maximum around the time 1800 μsec. The diffuse maximum at room temperature corresponds to the ASRO diffuse peak located at the 1,0.3,0 reciprocal-lattice position. The intensity distribution at room temperature is unchanged down to about 200 K. The diffuse maximum increased gradually below 200 K and finally reached the spectrum at 11 K. This has indicated that the spin state at room temperature was perfectly paramagnetic. In fact, the SQUID results have shown that the deviating temperature T_0 from the Curie-Weiss law was about 165 K. Since undoubtedly the nuclear diffuse intensity keeps the room-temperature state down to 11 K, the intensity difference between room temperature and 11 K is due to the magnetic diffuse scattering component. This method has already been employed for selecting the magnetic diffuse intensity in Cu-Mn,[8] Ag-Mn,[9] and Au-Fe (Ref. 22) alloys. The separated magnetic component includes elastic and inelastic scattering due to the TOF method using the white neutron beam without a monochromator or an energy analyzer. At the low temperature of 11 K, the magnetic component of Ag-20.8 at. % Mn alloy with the freezing temperature $T_g = 69$ K, was regarded as quasielastic intensity, cf. the fact that the diffuse intensity at 10 K from a Cu-Mn alloy with $T_g = 79$ K was almost given as elastic scattering by Werner, Rhyne, and Gotaas.[11] The temperature dependence of the magnetic diffuse peak intensity at the 1,0.3,0 position for Ag-20.8 at. % Mn has shown no anomalies in the amplitude and the half width around T_g. It is thought that this is due to the much broader energy resolution.

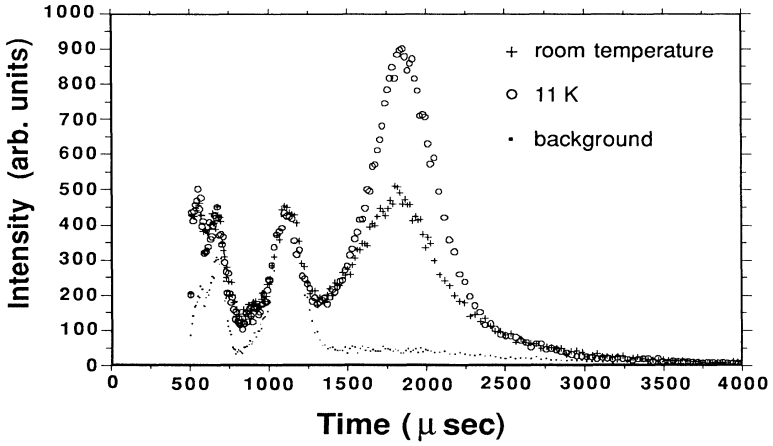

FIG. 7. TOF neutron spectra of Ag-20.8 at. % Mn alloy collected along the [1,0.3,0] direction at room temperature (+) and 11 K (○). The background spectrum displayed by dots was measured without the sample. The peak of the spectra around 1800 μsec corresponds to the diffuse maximum around the 1,0.3,0 reciprocal-lattice position. The difference between the intensity at room temperature and that at 11 K shows the contribution from the magnetic diffuse scattering. The peak around 1000 μsec has come from triple aluminum windows of a refrigerator.

The observed TOF spectra were normalized by the incident neutron spectrum obtained by incoherent scattering from a vanadium sample. The atomic and magnetic diffuse intensities were estimated by correcting for absorption, temperature factor, incoherent scattering, multiple scattering,[23] and paramagnetic scattering, and with the magnetic form factor of a Mn^{2+} ion.[24] They were converted into the absolute units, i.e., Laue unit for the atomic diffuse intensity and paramagnetic scattering unit for the magnetic diffuse intensity with consideration given to the mass of the Ag-20.8 at. % Mn alloy and that of the vanadium sample. The resolution conditions estimated by the full width at half maximum (FWHM) of 200 Bragg profiles were $0.018a^*$, $0.077a^*$, and $0.076a^*$ for horizontal, vertical, and radial directions, respectively. The resolution corrections for the vertical and radial directions were performed with a deconvolution procedure and their profiles. The atomic diffuse intensity distribution obtained by the neutron experiment corresponded to the x-ray result within about $\pm 10\%$ as shown in Fig. 8, where the atomic diffuse intensities along the $1,k,0$ reciprocal-lattice direction from both experiments are depicted. The corrected magnetic diffuse intensity map on the $(hk0)$ reciprocal-lattice plane is shown in Fig. 9, which exhibits sharp peaks at $1,0.28\pm0.01,0$ and $1,0.72\pm0.01,0$ positions with elongations to [1,0,0] and [0,0,1] directions, respectively. The FWHM of the diffuse peak at the 1,0.28,0 position was $0.10a^*$ for the [1,0,0] direction and $0.04a^*$ for the [0,1,0] and [0,0,1] directions.

B. MSRO Parameters

In this subsection, we describe the magnetic diffuse intensity in terms of ASRO and MSRO parameters. The spin-glass states in Ag-Mn alloys (Ag-20.0, 23.7 at. % Mn) are observed not to have any magnetic anisotropy in zero field.[1] Therefore, the classical Heisenberg model is applicable to represent the spin state in the present Ag-20.8 at. % Mn alloy. Under this model, the observed

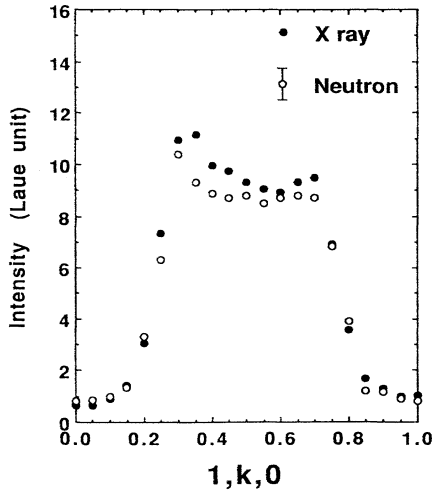

FIG. 8. The atomic diffuse scattering along $1,k,0$ reciprocal-lattice positions obtained by x-ray and neutron experiments. The resolution correction was performed to the neutron results.

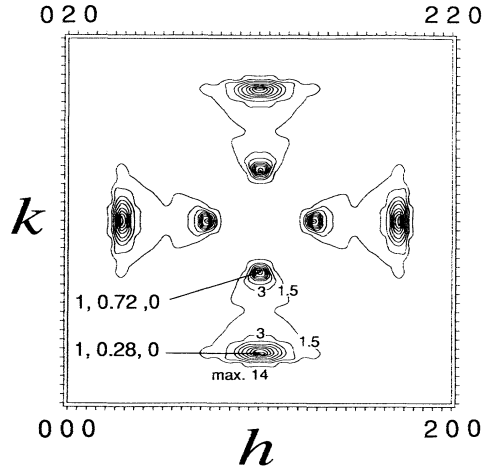

FIG. 9. The magnetic diffuse scattering of Ag-20.8 at. % Mn alloy on the $(hk0)$ reciprocal-lattice plane in the unit of the paramagnetic scattering intensity.

magnetic diffuse intensity is expressed as the paramagnetic scattering intensity modulated by the spin correlation as in the following:

$$I_{\text{mag-dif}}(q)=2/3(\gamma e^2/mc^2)^2 S(S+1)|f_{\text{Mn}}(\mathbf{q})|^2 \times \sum_u \sum_v \hat{\mathbf{S}}_u \hat{\mathbf{S}}_v \exp\{i\mathbf{q}(\mathbf{r}_u-\mathbf{r}_v)\} \ . \quad (1)$$

where f_{Mn} is the magnetic form factor of Mn spin, S is the angular spin momentum, and $\hat{\mathbf{S}}$ indicates the unit spin vector. The above equation without spin correlations at high temperature gives the paramagnetic scattering intensity. The coordinates u and v are only concerned with spin sites belonging to the Mn atoms which are allocated on the fcc lattice points with probability functions described by the ASRO parameters. With these functions, the summation of Eq. (1) is transformed to that over the general coordinates i and j as

$$\sum_u \sum_v \hat{\mathbf{S}}_u \hat{\mathbf{S}}_v \exp\{i\mathbf{q}(\mathbf{r}_u-\mathbf{r}_v)\} = \sum_i \sum_j (c\hat{\mathbf{S}}_i)(p_{ij}\hat{\mathbf{S}}_j)\exp\{i\mathbf{q}(\mathbf{r}_i-\mathbf{r}_j)\} \ , \quad (2)$$

where c is the content of Mn atoms and p_{ij} is the probability function for Mn-Mn atom pairs at the distance $\mathbf{r}_i-\mathbf{r}_j$. They are directly connected to the ASRO parameters as

$$p_{ij}=c+(1-c)\alpha_{lmn} \ . \quad (3)$$

From Eqs. (2) and (3), Eq. (1) can be expressed as

$$I_{\text{mag-dif}}(q)=2/3Nc(\gamma e^2/mc^2)^2 S(S+1)|f_{\text{Mn}}(\mathbf{q})|^2 \times \sum_{lmn} \{c+(1-c)\alpha_{lmn}\}\xi_{lmn}\exp(i\mathbf{q}\mathbf{r}_{lmn}) \ , \quad (4)$$

where N is the number of atoms, $\mathbf{r}_{lmn}=\mathbf{r}_i-\mathbf{r}_j$, and the ξ_{lmn} are the MSRO parameters, i.e., the spin correlation functions defined as

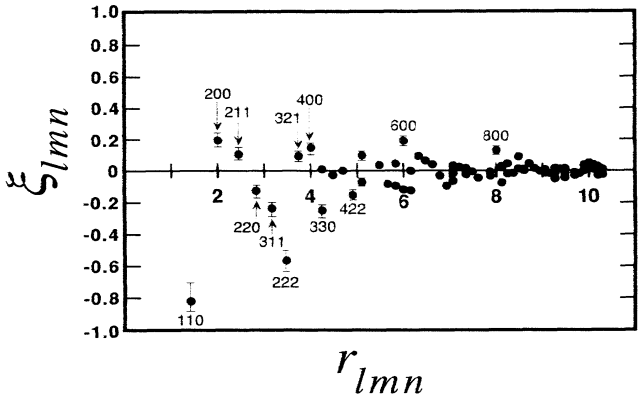

FIG. 10. The spin correlation function ξ_{lmn} of Ag-20.8 at. % Mn plotted against $r_{lmn}=(l^2+m^2+n^2)^{1/2}$, where l, m, and n are integers.

$$\xi_{lmn}=\langle \hat{\mathbf{S}}_0\hat{\mathbf{S}}_{lmn}\rangle \ . \tag{5}$$

A series of $\{c+(1-c)\alpha_{lmn}\}\xi_{lmn}$ values are taken by Fourier transform of the magnetic diffuse intensity. We are, therefore, able to get ξ_{lmn} with the use of ASRO parameters α_{lmn} obtained from the x-ray experiment. From the above procedures, the spin correlation function ξ_{lmn} was obtained as a function of the atomic distance r_{lmn} $[=(l^2+m^2+n^2)^{1/2}]$ as shown in Fig. 10. Positive or negative values of ξ_{lmn} correspond to the spin pairs at the distance r_{lmn} coupling ferromagnetically or antiferromagnetically, respectively. The first-nearest spin pairs were found to have strong antiferromagnetic coupling and the sign of ξ_{100} values along the $\langle 100\rangle$ direction, such as ξ_{200}, ξ_{400}, ξ_{600}, and ξ_{800}, are all positive, which means that the ferromagnetic linkings are presented along $\langle 100\rangle$ directions. The spin correlation length was estimated by reconstruction of the magnetic diffuse peak intensity, to be about $11a_0$, which is about two times longer than the atomic correlation length.

VI. DISCUSSION

A. Local spin structure and the relationship to the magnetic measurement results

Previous x-ray- diffraction and EXAFS studies gave only qualitative interpretations for the local atomic structure. The present quantitative analysis has been performed to understand the local arrangement of Mn atoms in Ag-Mn alloys more directly. Our structural models of the Ag-Mn alloys are as follows. Chains of Mn atoms along $\langle 100\rangle$ directions exist even in the lower Mn content alloys such as the Ag-13.3 at. % Mn alloy. With increasing Mn content, the population of chains increases and they become longer and longer. In the Ag-20.8 at. % Mn alloy, these chains connect with each other three-dimensionally as shown in Fig. 6(d). The result of the spin correlation function for this sample indicates that the local spin structure is strongly ruled by the local structure of Mn atoms. In particular, the ferromagnetic spin chains appeared on the Mn atom chains along $\langle 100\rangle$ directions due to the ferromagnetic interaction at the second-nearest-neighbor distance. Owing to these chains linking to the finite range, the ferromagnetic correlation could not develop the ferromagnetic long-range order. The ferromagnetic spin chains are connected with each other by the strong antiferromagnetic interactions at the first-nearest-neighbor distance.

As the Mn content increases further from 20.8 at. %, the local structure of Mn atoms changes abruptly. The decrease of the amplitude of ASRO parameters gives rise to the three-dimensional networks by first-nearest Mn-Mn atom pairs (red lines) as illustrated in Fig. 6(f). The ratio of second-nearest-neighbor Mn-Mn atom pairs to first-nearest ones is suddenly decreased as shown in Table III and the chains of Mn atoms along $\langle 100\rangle$ directions are shortened. It is noticed that their definite chainlike nature has been lost. We have found that these structural changes have been strongly related to the magnetic properties. In the Ag-28.1 at. % Mn alloy, the three-dimensional networks of the first-nearest Mn-Mn bonds drive the amplitude of magnetic susceptibility at T_g to decrease drastically due to the strong antiferromagnetic interaction between the first-nearest-neighbor Mn spins. The results of this structural change are also exhibited in the paramagnetic Curie temperature Θ. In the case of the local structure of Ag-20.8 and 13.3 at. % Mn alloys, the number of the ferromagnetic interactions between the second-nearest Mn pairs was greater in the local spin structure, and the summation over all spin bonds gave rise to the positive value. The sudden increasing of the intense antiferromagnetic interaction bonds in the Ag-28.1 at. % Mn turned Θ negative.

B. Origin of the diffuse peaks

Characteristic diffuse scattering can be interpreted in terms of the Fermi surface imaging theory proposed by Krivoglaz[25] and Moss.[26] Such an interpretation was given to the diffuse scattering observed from disordered alloys, e.g., Cu-Au,[26] Au-25 at. % Cu with an additional element of Pd or In,[27] Cu-Al,[28] Cu-Pd,[29,30] Cu-Pt,[29] Ag-Mg,[31,32] Au-Zn,[31] and Au-Pd.[31] Since the pair-interaction potential mainly originates from conduction electrons in these noble-metal based alloys, the diffuse scattering reflects the flat portions around $\langle 1,1,0\rangle$ directions of the Fermi surface. Although there are no apparent diffuse streaks around the $\langle 1,1,0\rangle$ direction for the present Ag-Mn alloy, diffuse maxima appear around $1,0.5\pm\delta,0$ and its equivalent positions, and δ depends on the Mn content. As the $3d$ electrons of Mn atoms are contained in this alloy, it is more complicated to apply the Fermi surface imaging idea in understanding the present diffuse patterns. The peak positions of the atomic and magnetic diffuse scatterings were observed by previous authors in the Cu-Mn (Refs. 8, 10, and 33) and Ag-Mn (Ref. 9) alloys which were displayed in Fig. 11 with our present results. Although the atomic diffuse peak is not located exactly at the magnetic one, the composition dependence of the peak position is regarded to be controlled under the Fermi surface effect with increasing of

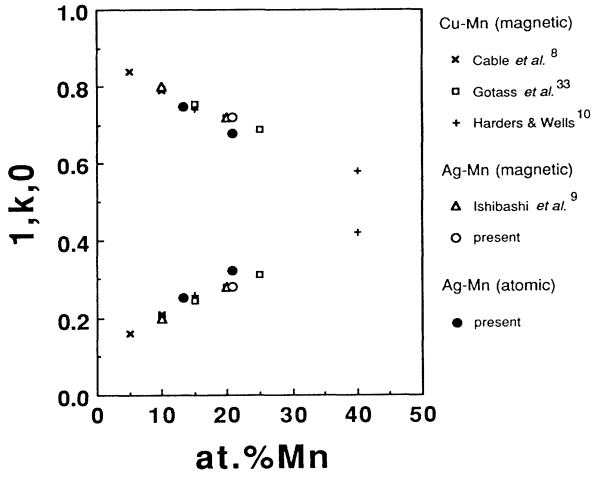

FIG. 11. The positions of atomic and magnetic diffuse peaks as a function of Mn concentration for Cu-Mn and Ag-Mn alloys.

the ratio of the number of electrons per an atom (e/a). In particular, the magnetic diffuse peak position is thought to be varied by the Fermi surface effect via RKKY interaction under which Mn spins are connected with a modulation period $2k_F$ beyond the atomic correlation range. The direct verification for the above discussions will be performed by making a comparison between the Fermi surface of Ag and Ag-Mn alloys around the $\langle 1,1,0 \rangle$ direction with the use of the positron annihilation method. The Fermi surface effect of the Ag-20.8 at. % Mn alloy will also be confirmed indirectly by measuring the shifting of the atomic and magnetic diffuse peaks which would take place with doping of small amounts of In^{3+} or Cd^{2+} ions instead of Ag^{+} ions under the fixed Mn contents.

C. Summary

In contrast to the distinct development of ASRO in the Ag-Mn alloys, the Cu-Mn alloys are known to have only a weak ASRO effect over the large concentration range,[5,21,34] which bring a nearly random fashion of Mn atoms.[35] In spite of this difference in the local structure of Mn atoms between the two alloy systems, the magnetic diffuse peak in the present Ag-Mn alloy exhibits quite similar three-dimensional shape[8] and good coincidence of peak positions and its concentration dependence[9] to the Cu-Mn alloy. This indicates the existence of the same longer-range spin correlation for both alloys, which may be realized by the same Fermi surface effect via RKKY interaction due to the possession of the similar Fermi surface in pure Ag and Cu. On the other hand, the short-range spin structure formed on their own ASRO differed significantly. This disagreement appeared in the intensity distribution around the 1,0.5,0 reciprocal-lattice position. The atomic diffuse intensities of the Cu-Mn alloys with ferromagnetic clusters contribute to make the same patterns on the magnetic ones around the 1,0.5,0 position.[8] The lower intensity distribution in the present Ag-Mn alloy is caused by the absence of the ferromagnetic clusters. Although these two alloys have very different local atomic and spin structures, they are known to show similar spin-glass properties.[1] We found a big change in the local structure between Ag-20.8 at. % Mn and Ag-28.1 at. % Mn, which affected the peak value of susceptibility and the paramagnetic Curie temperature, however, the freezing temperature was observed to have a common linearlike function with the Mn content. Accordingly, it seems that the freezing temperature is not controlled by the local spin structure, but mainly related to the density of Mn spins. As the longer-range spin correlations by RKKY interactions are not related to the local structures, we think that their interconnections bring about the spin-glass freezing below the deviating temperature T_0 from the Curie-Weiss law. We believe that the longer-range spin correlations are not able to grow without any confusion with the local spin structures, and finally they fall into competing states by themselves inside the atomic short-range ordered region, where they cannot change their spin directions into lower energetic states any more. The coexistence of short-range spin structures and longer-range spin correlation is thought to be an intrinsic nature for the spin-glass freezing.

ACKNOWLEDGMENTS

The authors wish to thank Dr. Y. Tsunoda of Osaka University for his advice in growing single crystals and Dr. E. Kita of University of Tsukuba for his support in measuring the magnetic susceptibilities. We are also grateful to K. Iwai of the machine shop of National Laboratory for High Energy Physics for his help in constructing the neutron four-circle goniometer and to K. Nishida of Chemical Analysis Center of University of Tsukuba for his assistance in EPMA. This work was supported by the Grant-in-Aid for Scientific Research from the Ministry of Education, Science and Culture.

[1] J. S. Kouvel, J. Phys. Chem. Solids **21**, 57 (1961).
[2] H. Bouchiat, E. Dartyge, P. Monod, and M. Lambert, Phys. Rev. B **23**, 1375 (1981).
[3] H. Bouchiat and E. Dartyge, J. Phys. (Paris) **43**, 1699 (1982).
[4] E. Dartyge and A. Fontaine, J. Phys. F **14**, 721 (1984).
[5] P. Wells and J. H. Smith, J. Phys. F **1**, 763 (1971).
[6] S. A. Werner and J. W. Cable, J. Appl. Phys. **52**, 1757 (1981).
[7] J. W. Cable, S. A. Werner, G. P. Felcher, and N. Wakabayashi, Phys. Rev. Lett. **49**, 829 (1982).
[8] J. W. Cable, S. A. Werner, G. P. Felcher, and N. Wakabayashi, Phys. Rev. B **29**, 1268 (1984).
[9] K. Ishibashi, Y. Tsunoda, N. Kunitomi, and J. W. Cable, Solid State Commun. **56**, 585 (1985).
[10] T. M. Harders and P. Wells, J. Phys. F **13**, 1017 (1983).
[11] S. A. Werner, J. J. Rhyne, and J. A. Gotaas, Solid State Commun. **56**, 457 (1985).
[12] T. B. Massalski, *Binary Alloy Phase Diagram* (American Society for Metals, Metals Park, OH, 1986), Vol. 1, p. 43.
[13] N. Ahmed and T. J. Hicks, Solid State Commun. **15**, 415 (1974).

[14]G. Mozurkewich, J. H. Elliott, M. Hardiman, and R. Orbach, Phys. Rev. B **29**, 278 (1984).
[15]P. Gibbs, T. M. Harders, and J. H. Smith, J. Phys. F **15**, 213 (1985).
[16]B. Borie and C. J. Sparks, Acta Crystallogr. Sec. A **27**, 198 (1971).
[17]R. O. Williams (unpublished).
[18]H. Suzuki, J. Harda, M. Matsui, and K. Adachi, Acta Crystallogr. Sec. A **38**, 522 (1982).
[19]K. Ohshima, N. Iwao, and J. Harada, J. Phys. F **17**, 1769 (1987).
[20]K. Koga and K. Ohshima, J. Phys. Condens. Matter **2**, 5647 (1990).
[21]M. Hirabayashi, M. Koiwa, S. Yamaguichi, and K. Kamata, J. Phys. Soc. Jpn. **45**, 1591 (1978).
[22]J. W. Cable, G. Parette, and Y. Tsunoda, Phys. Rev. B **36**, 8467 (1987).
[23]I. A. Blech and B. L. Averbach, Phys. Rev. **137**, 1113 (1965).
[24]L. M. Corliss, N. Elliot, and J. Hastings, Phys. Rev. **104**, 924 (1956).
[25]M. A. Krivoglaz, *Theory of X-ray and Thermal Neutron Scattering by Real Crystals* (Plenum, New York, 1969).
[26]S. C. Moss, Phys. Rev. Lett. **22**, 1108 (1969).
[27]S. Hashimoto and S. Ogawa, J. Phys. Soc. Jpn. **29**, 710 (1970).
[28]R. O. Scattergood, S. C. Moss, and M. B. Bever, Acta Metall. **18**, 1087 (1970).
[29]K. Ohshima and D. Watanabe, Acta Crystallogr. Sec. A **29**, 520 (1973).
[30]K. Ohshima, D. Watanabe, and J. Harada, Acta Crystallogr. Sec. A **32**, 883 (1976).
[31]K. Ohshima and D. Watanabe, Acta Crystallogr. Sec. A **33**, 784 (1977).
[32]K. Ohshima and J. Harada, Acta Crystallogr. Sec. B **42**, 436 (1986).
[33]J. A. Gotaas, J. J. Rhyne, and S. A. Werner, J. Appl. Phys. **57**, 3404 (1985).
[34]J. R. Davis, S. K. Burke, and B. D. Rainford, J. Magn. Magn. Mater. **15-18**, 151 (1980).
[35]H. Suzuki and J. Harada, J. Magn. Magn. Mater. **31-34**, 69 (1983).

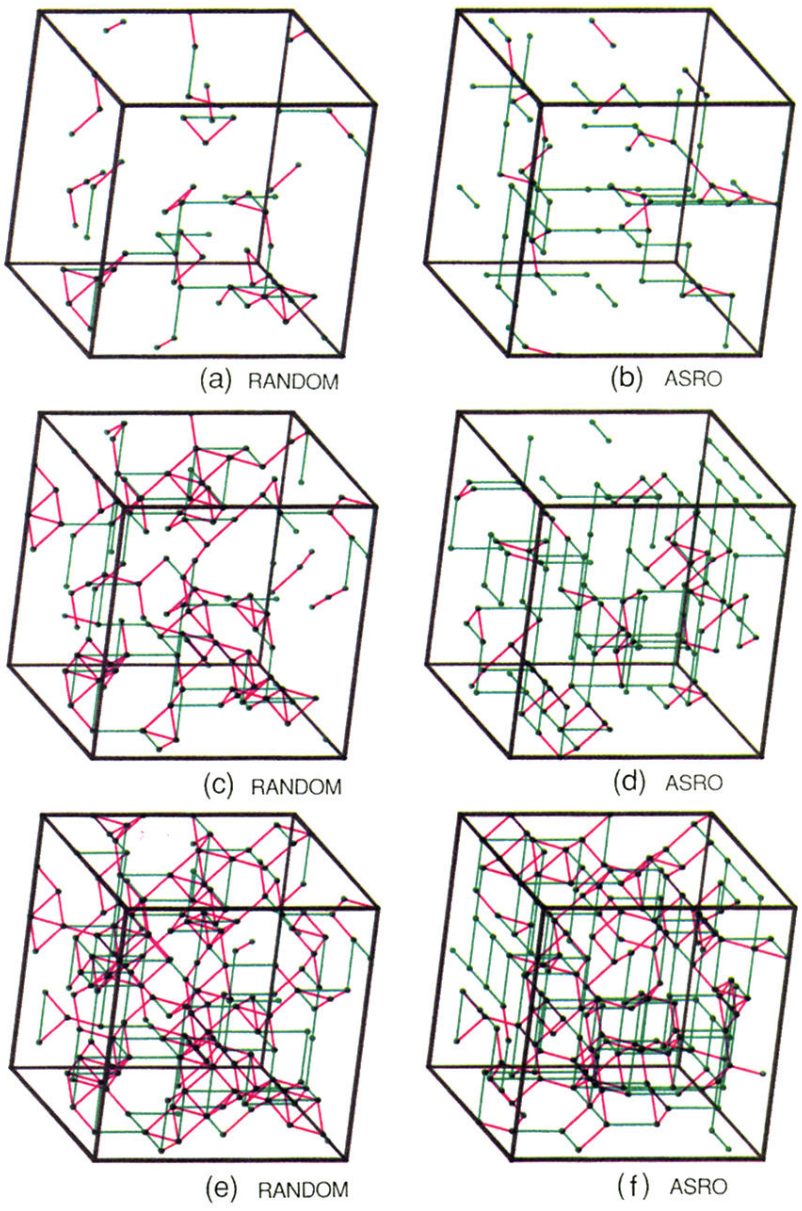

FIG. 6. Three-dimensional distribution of Mn atoms simulated on $5\times5\times5$ fcc unit cells; (a), (c), and (e) for the ideally disordered state of Ag-13.3, Ag-20.8, and Ag-28.1 at. % Mn alloys, respectively, and (b), (d), and (f) for the observed ASRO structures of Ag-13.3, Ag-20.8, and Ag-28.1 at. % Mn alloys, respectively. Only Mn atoms are represented by circles and they are linked together by red and green solid lines which are first- and second-nearest neighbors to each other in a fcc lattice.